

OPEN ACCESS

Elucidating Copper Dissolution Phenomenon in Li-Ion Cells under Overdischarge Extremes

To cite this article: Conner Fear *et al* 2018 *J. Electrochem. Soc.* **165** A1639

View the [article online](#) for updates and enhancements.



Elucidating Copper Dissolution Phenomenon in Li-Ion Cells under Overdischarge Extremes

Conner Fear,¹ Daniel Juarez-Robles,^{1,*} Judith A. Jeevarajan,^{2,**,z} and Partha P. Mukherjee^{1,z}

¹School of Mechanical Engineering, Purdue University, West Lafayette, Indiana, USA

²Electrochemical Safety, Underwriters Laboratories Inc., Northbrook, Illinois, USA

The mechanisms driving the thermo-electrochemical response of commercial lithium-ion cells under extreme overdischarge conditions (< 0.0 V) are investigated in the context of copper dissolution from the anodic current collector. A constant current discharge with no lower cutoff voltage was used to emulate the effects of forced overdischarge, as commonly experienced by serially connected cells in an unbalanced module. Cells were overdischarged to 200% DOD (depth of discharge) at C/10 and 1C rates to develop an understanding of the overdischarge extremes. Copper dissolution began when a cell reached its minimum voltage level (between -1.3 V and -1.5 V), where the anode potential reached a maximum value of ~ 4.8 V vs. Li/Li^+ . Deposition of copper on the cathode, anode, and separator surfaces was observed in all overdischarged cells, verified with EDS/SEM results, which further suggests the formation of internal shorts, although the cell failures proved to be relatively benign. The maximum cell surface temperature during overdischarge was found to be highly rate-dependent, with the 1C-rate cell experiencing temperatures as high as 79°C . Concentration polarization and solid electrolyte interphase (SEI) layer breakdown prior to the initiation of copper dissolution are proposed to be the main sources of heat generation during overdischarge.

© The Author(s) 2018. Published by ECS. This is an open access article distributed under the terms of the Creative Commons Attribution Non-Commercial No Derivatives 4.0 License (CC BY-NC-ND, <http://creativecommons.org/licenses/by-nc-nd/4.0/>), which permits non-commercial reuse, distribution, and reproduction in any medium, provided the original work is not changed in any way and is properly cited. For permission for commercial reuse, please email: oa@electrochem.org. [DOI: 10.1149/2.0671809jes]



Manuscript submitted April 9, 2018; revised manuscript received May 21, 2018. Published June 5, 2018.

The market for lithium-ion batteries (LIBs) has experienced rapid growth in recent years, as their high power, high energy, and efficient reversibility make them attractive for numerous energy storage applications.¹ In particular, interest in powering electric vehicles (EVs) and portable electronics have spurred the development of a wide variety of cells with increased energy densities.² Unfortunately, the increased energy storage capabilities of lithium-ion cells have been overshadowed by the frequent occurrence of accidents, revealing several safety concerns that require further investigation.³ For instance, UPS Flight 6 was a Boeing 747 cargo plane that was believed to have crashed in 2010 due to the autoignition of the contents of a cargo pellet containing a significant number of lithium type batteries.⁴ Samsung was forced to recall nearly 1 million Galaxy Note 7 phones in September 2016 after numerous reports of the devices going into thermal runaway during charging or use.⁵ It was later revealed that the issue stemmed from two independent cell design flaws by the two different manufacturers, causing them to short circuit. In February 2017, a Dell Inspiron laptop powered by a LIB violently combusted while charging and proceeded to burst into flames three more times after being unplugged.⁶ These examples illuminate the fragility of the Li-ion chemistry and demonstrate the necessity of understanding the response of Li-ion cells to abnormal conditions.⁷⁻⁹

Commercial LIBs typically specify a voltage range (~ 2.5 – 4.2 V for a single cell) for safe operation in order to prevent undesirable side reactions from occurring in the cell. A condition known as overdischarge occurs when a cell is discharged below the manufacturer's recommended lower voltage limit. Overdischarge is becoming an increasingly common issue as greater numbers of cells are being connected in parallel-series configuration, as is the case in systems requiring high voltages, such as EVs.¹⁰ When placed in a battery arrangement, the voltage of individual cells should be monitored in order to keep them in balance and within the manufacturer's specification. Slight differences in the manufacturing of cells can cause some cells to have less capacity than others in the series.¹¹ Nevertheless, when the module is discharging, the cells with lower capacity are demanded to deliver the same amount of energy as other cells. When lower capacity cells in an unbalanced module discharge beyond their recommended lower voltage limit, overdischarge occurs and permanent

capacity fade or failure can be caused.¹² Additionally, overdischarge below the manufacturer specified low voltage limit will result in the dissolution of the copper anodic current collector, which can deposit on internal cell components and induce an internal short.^{13,14} Typically, internal shorts due to an overdischarge condition are benign, leading to a dead cell in a fail-safe mode.¹⁵ However, the dissolution of copper from the anode current collector causes additional issues such as delamination of the anode and the deposition of copper on the surfaces of the cathode, separator and anode, which hinders the flow and intercalation/deintercalation of lithium-ions during charge and discharge.¹⁵ This causes lithium ions to deposit as lithium metal rather than intercalating into the anode electrode, as the surface of the anode is covered with copper.

While many studies have investigated the effects of overdischarge in LIBs below the manufacturer's recommended lower cutoff voltage,¹⁶ few prior studies have focused on overdischarge below 0.0 V. Kishiyama et al. studied the effects of 0.0 V overdischarge on Li-ion cells whose anodes used current collectors made of either titanium or copper.¹⁷ They demonstrated that the dissolution of copper is the main cause of capacity loss in cells under this condition. It was also shown that the Solid Electrolyte Interphase (SEI) layer could break down if the anode potential exceeds 3.5 V vs. Li/Li^+ . Mao demonstrated that anode potential can reach as high as 3.8 V when overdischarging a Li-ion cell to 0.0 V.¹⁸ Therefore, it is possible that both copper dissolution and breakdown of the SEI layer are causes of capacity loss during the overdischarge process. A study performed by Li et al. observed swelling in a LiCoO_2 -based pouch cell that was overdischarged to 0.0 V, using gas chromatography to detect and quantify the gases that caused the swelling.¹⁶ Carbon dioxide, carbon monoxide, and methane were found to be the most abundant gases in the overdischarged cells. The authors propose that the carbon dioxide and carbon monoxide were produced from the decomposition of the SEI.

Guo et al. proposed using extreme overdischarge as a method to consistently induce internal shorting in lithium-ion cells, caused by the dissolution of copper and the creation of electrical shunts when it was redeposited on electrode surfaces.¹³ Cells were subjected to extreme overdischarge of varying degrees before recharge was attempted. It was found that for cells in which the discharge was terminated before 112% DOD, full recharge could be achieved with only minor side effects, while cells that were terminated beyond 114.5% DOD could not be recharged back to full. The authors of this study also note that

*Electrochemical Society Student Member.

**Electrochemical Society Member.

^zE-mail: pmukherjee@purdue.edu; Judy.Jeevarajan@ul.com

increasing the capacity ratio of the anode to the cathode can delay the DOD at which copper dissolution begins.

A study by He et al. investigated the failure mode of commercial 18650 LiFePO₄ cells subjected to repeated overdischarge to DODs from 105% to 120%.¹⁰ The proposed failure mode from this study is the gradual formation of copper bridges through repeated cycling, which cause micro-shorting and self-discharge. They also performed cyclic voltammetry tests on copper electrodes in LiPF₆ electrolyte to determine precise oxidation and reduction potentials for copper. The oxidation and reduction potentials of the Cu to Cu⁺ reaction were measured at 3.92 and 3.28 V, respectively, while the potentials of the Cu⁺ to Cu²⁺ reaction were measured at 4.17 and 3.19 V.¹⁰ Because these tests were performed ex-situ, the measured potentials cannot directly predict the in-situ oxidation and reduction potentials of copper at graphite anodes and lithium metal oxide cathodes. To track the potential evolution of each electrode throughout a 1C-rate overdischarge to 120% DOD, a modified three-electrode 18650 cell, using lithium metal as the reference electrode, was employed. The anode potential increased from -0.5 to 4.5 V vs. Li/Li⁺ during the test, while the cathode potential decreased from 3.80 to 3.18 V vs. Li/Li⁺.¹⁰

Kasnatscheew et al. analyzed the potential development and interactions between electrodes in a three-electrode Swagelok cell with an NMC cathode, graphite anode, and Li metal reference electrode throughout a deep overdischarge phase.¹⁹ A characteristic potential plateau at ~3.56 V was detected at the graphite electrode due to the copper oxidation process at the current collector. The constant anode potential following the onset of copper oxidation indicates that the process continued throughout the remaining discharge phase. The time shifted potential plateau observed at the positive electrode, was attributed to the competitive reaction between the conventional lithiation reaction and the parasitic Cu plating reaction.

Overdischarge of 18650 cells in a parallel arrangement was studied by Nemanick et al. in a test to simulate an electronic control failure.¹⁵ Cells were overdischarged via successive cycling in which 60% of the nominal capacity was discharged and only 90% of the removed charge was returned during recharge in each cycle. All cells appeared to develop shorts after 9 cycles. Even so, cell temperatures peaked at around 40°C during cycle 9 and returned to near-ambient temperatures for the cycles following the shorting, showing the fail-safety of this form of cell abuse. Cross-sectional SEM confirmed that dendrites had formed on the cathode surface and penetrated through the separator, often visibly connecting through to the anode.¹⁵

In this study, the response of commercial 18650 LIBs to a single deep overdischarge is examined in order to elucidate the mechanisms that lead to cell failure under this condition. A constant current discharge phase with no lower cutoff voltage is used to overdischarge the cell to 200% DOD so that a thorough electrochemical analysis of the entire overdischarge condition could be performed. Differential voltage analysis is used to study the copper dissolution reactions as a function of DOD. Destructive physical analysis (DPA) was employed to visually inspect damage in the cell, and the morphological changes on the electrodes were studied by analyzing cell components using micrographic (SEM) and spectroscopic (EDS) techniques.

In order to decouple the behaviors of the anode and cathode and to examine the interactions between the electrodes during extreme overdischarge, a series of half cell tests were performed. Electrodes harvested from the commercial 18650 cells are used to construct coin-type half cells with graphite and NCA. Half cell tests can provide useful information on the electrochemical behavior of an electrode, as they place the electrode under study opposite an electrode of known potential. Although the half cell analysis cannot account for any interactions that occur between electrodes in the full cell overdischarge, it enables an in-depth analysis of the reactions that occur at each electrode at different potentials and DODs. Since no copper current collector is present in the NCA/Li half cells, the deposition of copper on the NCA surface cannot be studied with this test, but other effects of overdischarge on the cathode can be examined without interference. The results of the half cell tests and the commercial full cell test will provide a complete picture of the reactions occurring during extreme

overdischarge of Li-ion cells, which will permit the elucidation of the mechanisms causing cell failure in this way.

Experimental

Commercial Panasonic NCR18650B cylindrical cells, obtained from a reputable vendor, were used in this study. The rated capacity of these cells is 3350 mAh at 25°C when discharged at a C/5 rate. The manufacturer-recommended voltage window is 2.5–4.2 V. The cathode active material is LiNi_{0.8}Co_{0.15}Al_{0.05}O₂ (NCA, nickel cobalt aluminum oxide) and the anode active material is graphite (C), with aluminum and copper foil as current collectors, respectively. The separator is composed of polypropylene (PP) and polyethylene (PE) with an oxide-polymer composite layer of alumina (Al₂O₃).²⁰ Cell voltage and electrical current were controlled and recorded by an Arbin-BT2000 battery cycler. Temperature measurements were recorded from a K-type thermocouple (Omega) attached to the exterior surface of the cell.

The cell was conditioned by charging and discharging two times, measuring the full cell capacity and internal resistance on the second cycle at 50% of the Depth of Discharge (DOD). Charging was performed under a constant current (CC) mode at a C/20-rate up to 4.2 V, followed by a constant voltage (CV) charge at 4.2 V until current fell below 0.05 A. Discharging was performed under CC conditions at a C/20 rate to a cutoff voltage of 2.5 V. Internal resistance was measured during the discharge phase at 50% SOC by applying a short current pulse at 1.5C for 100 ms. The cell was then fully charged to 4.2 V and allowed to rest.

To perform the overdischarge test, the cell was once again charged, discharged, and charged, this time at C/10 (335 mA), in order to ensure a 0% DOD at the beginning of the test. The cell was then subjected to a constant current discharge phase with no lower cutoff voltage, inducing extreme overdischarge. The discharge was allowed to continue until a 200% DOD was reached. Overdischarge was performed at rates of C/10 (335 mA) as well as 1C (3350 mA) to determine the possible effect of discharge rate on cell response during the process. The voltage and surface temperature of the cell were monitored and recorded throughout the test via the battery cycler.

Electrodes were harvested from a fresh Panasonic NCR18650B cell and used to construct 2300-type coin cells. Because the electrodes from the cylindrical cell are double-sided coated, the active material on one side had to be removed to expose the foil current collector. This was achieved by applying drops of isopropyl alcohol to the electrode surfaces and carefully scraping off the active material with a scalpel. Two graphite half cells were created using the anode from the fresh 18650 cell and the procedure described in Reference 21. These cells were conditioned by cycling at C/10 rate between 0.1–2.5 V vs. Li/Li⁺. After the second discharge to 0.1 V, one cell was overcharged at C/10 and the second half cell at 1C-rate with no upper cutoff voltage to 200% DOD, emulating the overdischarge of the anode in a full cell. Two NCA half cells were created from the cathode material and were conditioned by cycling at C/10-rate between 3.5–4.2 V. After the second charge to 4.2 V vs. Li/Li⁺, the cells were overdischarged independently at C/10 and 1C-rate with no lower cutoff voltage to 200% DOD.

Destructive physical analysis was performed on the overdischarged cell to determine what damage had been caused to cell components. Cells were disassembled within a sealed argon glove box (MBraun) for safety and to prevent reactions with the environment from affecting interior components. After performing DPA, scanning electron microscopy (SEM) and energy-dispersive X-ray spectroscopy (EDS) were performed on representative anode and cathode samples to examine the electrode surfaces after overdischarge abuse and to verify that the material deposited on the cathode surface is copper, dissolved from the anodic current collector.

Results and Discussion

Most off-the-shelf commercial cells are shipped at lower states of charge, typically at 30% DOD. The cells may be in storage for an

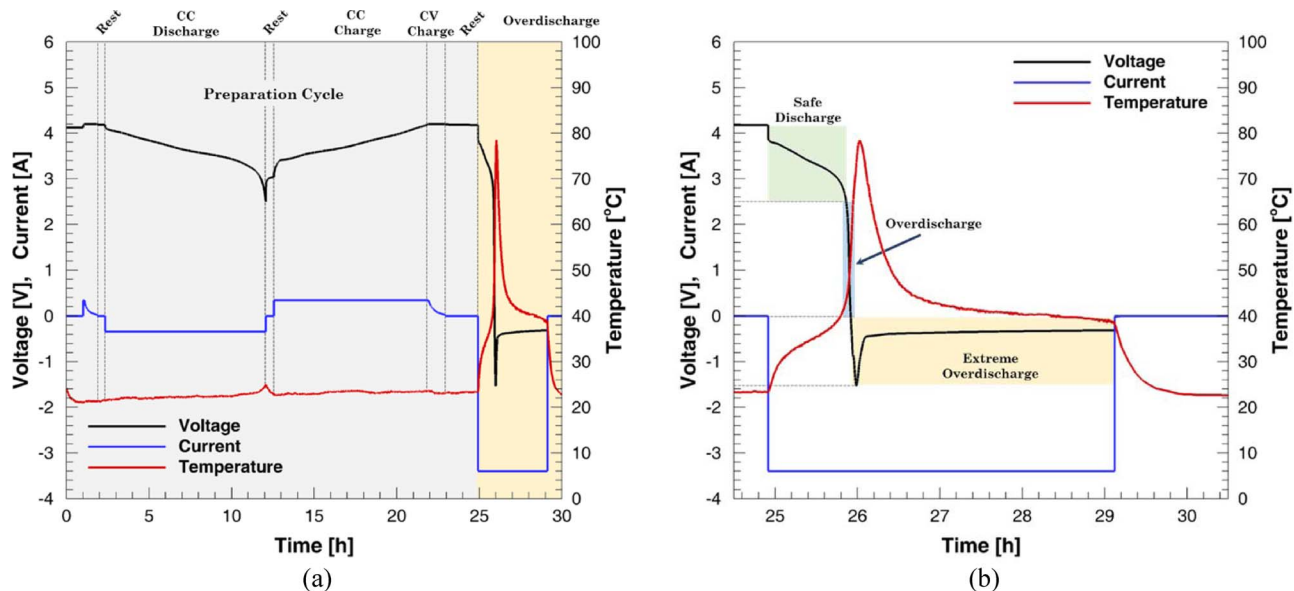


Figure 1. Experimental protocol for the overdischarge test at 1C discharge rate. The test consists of two steps: a preparation (CC discharge and CCCV charge at C/10 rate) and then the overdischarge process (CC discharge at 1C-rate). The preparation test ensures the cell to be fully charged prior the final overdischarge process, which is held for more than 3 hours.

indefinite time before they are sold and hence at least two conditioning cycles were performed on all the cells before other tests were conducted. The discharge capacity obtained in the first full cycle was 3330 mAh, which was slightly smaller than the rated capacity of the cell (3350 mAh). The 0% DOD was defined as the charge capacity obtained at the end of the CCCV charging from the conditioning test. The average internal resistance of the cells was 45 m Ω .

The protocol used in the experimental test for the 1C overdischarge is shown in Figure 1. The protocol ensures the cell to be fully charged prior the overdischarge test. At 2.5 V, which is the manufacturer-recommended lower cutoff voltage, the discharge capacity at a 1C-rate is 3214 mAh. This voltage range is considered a safe voltage window where the cell can be cycled with a long lifespan. If the cell is discharged below 2.5 V without going below 0.0 V, the cell is overdischarged, leading to electrolyte degradation and SEI decomposition.¹⁶ For the 1C test to 0.0 V, a discharge capacity of 3401 mAh was obtained. After that, the cell was driven to an extreme overdischarge condition (below 0.0 V) until the cell reached a 200% DOD.

The voltage profile for the overdischarge test can be roughly divided into four stages as shown in the differential voltage plot for the C/10 overdischarge test in Figure 2a. In Stage I, the voltage dropped rapidly from an inflection point in the voltage curve around 1.8 V to a distinct platform at about -1.0 V. In Stage II, the voltage continued to fall to its minimum value of -1.3 V. Stage III showed an increase in voltage with significant fluctuations, while in Stage IV, the voltage increased asymptotically to -0.23 V with very little fluctuation. An analogous examination of the 1C rate overdischarge test showed that Stage I, II, III, and IV started at 1.2 V, -0.9 V, -1.5 V, and -1.3 V, respectively. At the end of the extreme overdischarge, the asymptotic voltage reached for the 1C trial was -0.3 V. Note that while the voltage levels of these points vary with the discharge rate, the characteristic trend of the voltage profile is consistent for all tests performed on this type of cell. In order to facilitate the stage limits identification, the voltage vs. DOD plot were contrasted with its corresponding first and second order differential voltage curves (see Figure 2). The peak maximum voltage values were identified as the zeros of the first order differential voltage plot. The plateau voltages with changes in concavity were identified using the zeros of the second order differential voltage plot.

The voltage decline in Stage I, from Figure 2a, is driven primarily by the increasing potential of the anode, as the overall capacity of

the cathode is always designed to be lower than that of the anode in commercial cells in order to avoid possible lithium plating and dendrite formation on the anode during charging.¹¹ Deintercalation of the remaining Li⁺ ions from the anode and their introduction back into the cathode rapidly increase the anode potential throughout Stage I and gradually decrease the cathode potential. Stage I begins at an inflection point in the voltage curve around 1.8 V, which signifies the initiation of SEI decomposition. This inflection point is also evident in the graphite half cell voltage curve, shown in alignment with the full cell curve in Figure 3. According to Kishiyama et al., SEI breakdown can occur when the anode voltage reaches ~3.5 V or higher and can generate gases and heat within the cell.¹⁷ This process, which occurs throughout Stages I and II, exposes the chemically reactive surface of graphite to the electrolyte, further increasing the anode voltage and decreasing the voltage of the cell. As Stage I continues, another inflection point at ~0.0 V indicates the point at which the cathode potential begins to fall rapidly due to a lack of interstitial site availability and the buildup of a concentration gradient of Li in the NCA. The falling cathode potential and rising anode potential cause the full cell voltage to decrease until a plateau is reached at the end of Stage I. This brief plateau was also observed in the NCA half cell tests (see Figure 3), and indicates the introduction of new Li-rich phases in the cathode structure to accommodate the excess Li being forced into it. The volumetric expansion of NCA to incorporate these phases can cause cracking and permanently damage the cathode microstructure.

During Stage II, the rising potential of the anode dominates the full cell voltage behavior, as the cathode potential remains relatively constant. The anode potential continues to rise until it is high enough to overcome the overpotential required for copper dissolution. The oxidation potential of Cu to Cu⁺ was measured ex-situ by He et al. using cyclic voltammetry to be 3.92 V vs. Li/Li⁺ in LiPF₆ electrolyte.¹⁰ In this work, the Cu to Cu⁺ oxidation potential was measured in-situ using Cu/Li half cells to be 3.54 V at C/10 (3.60 V at 1C) and almost no initial peak for reaction overpotential was present. The difference between the in-situ and ex-situ measurements can be accounted for by the closer proximity of electrodes to each other in the in-situ tests, leading to a reduced effect of electrolyte resistance. In the case of the graphite/Li half cells, shown in Figure 3, the anode potential consistently reached a peak around 4.8 V, indicating the requirement of a large overpotential to initiate copper dissolution when a graphite coating is present. This is possibly due to charge transfer resistance of the Cu⁺ ions, as they are too large to travel directly through the

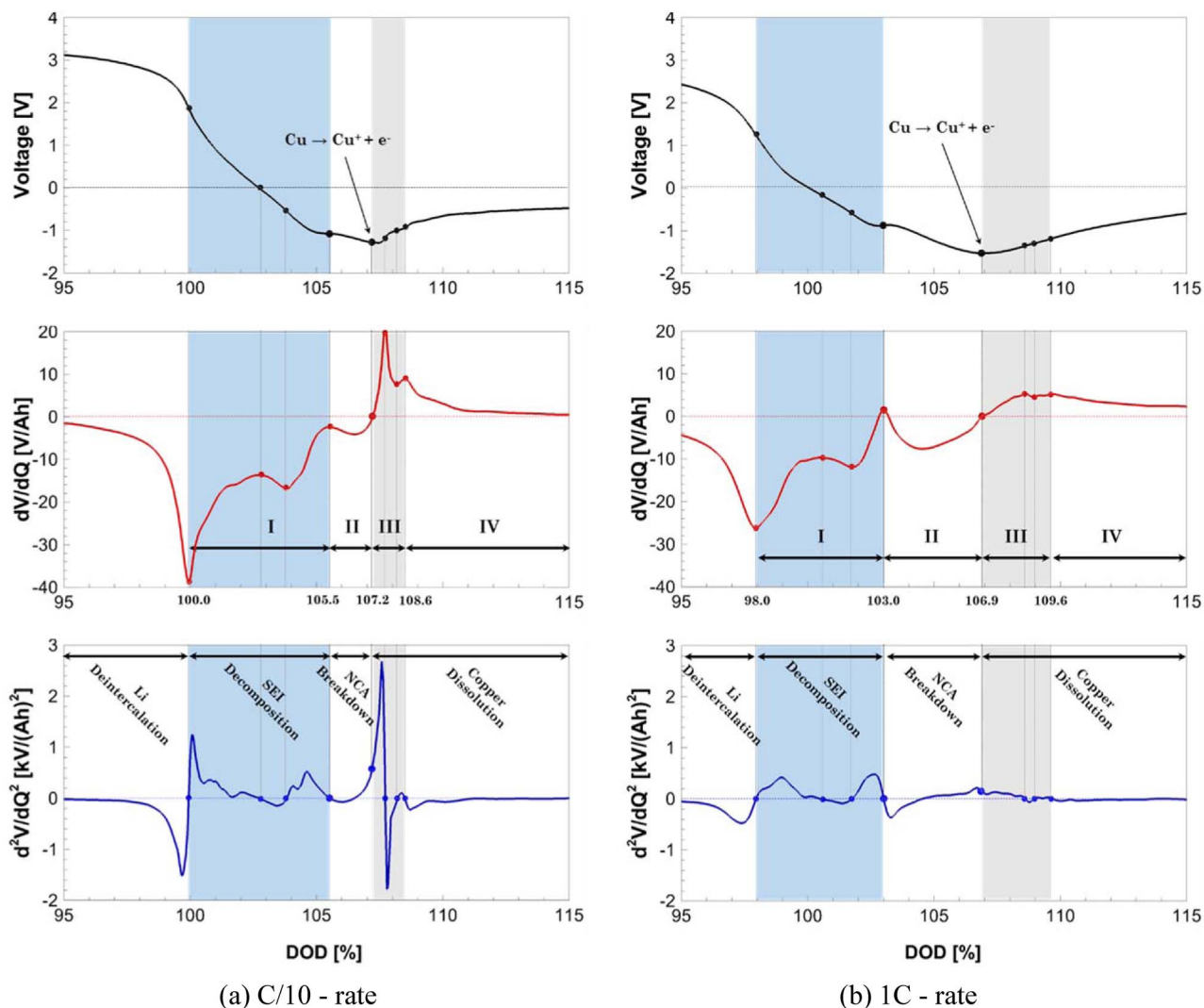


Figure 2. Zero-th (V vs. DOD), first (dV/dQ vs. DOD) and second (d^2V/dQ^2 vs. DOD) order differential voltage as a function of DOD. In the voltage plot, the DOD at which copper dissolution dominates the performance of the cell is highlighted. Zeros for the first and second differential voltage allow tracking the electrochemical changes – concavity shifts – within the cell. The side reactions, indicated in the differential voltage plot, can be identified by the four (I, II, III, IV) overdischarge stages.

graphite and must travel primarily around the edges of the electrodes. In the full cell analysis, copper oxidation begins when it reaches its minimum value at the end of Stage II, identified by a zero in the differential voltage curve (see Figure 2).

Following the onset of the copper dissolution reaction, the anode potential falls as the overpotential for the reaction is relieved. The anode potential decreases rapidly throughout Stage III, while the cathode potential gradually decreases at a slower rate, resulting in an increase in the full cell voltage. According to the ex-situ measurements of He et al., Cu^+ ions dissolved in the electrolyte will reduce to metallic copper at around 3.19 V.¹⁰ In these tests, the cathode potential fell below this value prior to the onset of dissolution, so the large time-shift between the start of copper oxidation at the anode and copper reduction at the cathode reported by Kasnatscheew et al. is not observed. Although the NCA/Li half cell results in Figure 3 show a continuous decrease in potential with increasing DOD, this result does not account for the presence of copper ions in the electrolyte. Therefore, the NCA/Li half cell voltage curve does not accurately represent the full cell cathode behavior after the start of Stage III. When the reduction and intercalation of Li at the NCA surface is competed by the reduction and deposition of Cu, the intended Li reaction is kinetically hindered and the cathode potential slightly increases.¹⁹ Therefore, the

start of copper deposition at the cathode can be associated with the minimum cathode potential in the full cell. Stage III ends at an inflection point, where the cathode reaches its minimum potential and copper deposition begins to occur.

Stage IV is characterized by a plateau in the anode potential at ~ 3.54 V for the remainder of the overdischarge, indicating the continuing dissolution of copper from the current collector.^{10,19} The voltage rise in Stage IV is driven by the increasing potential of the cathode, as the overpotential for copper reduction is relieved and copper ions compete with lithium ions to be reduced at the electrode surface. The gradual rise in voltage can be attributed to inhomogeneous blockage of the cathode's reactive surface by copper deposits, as well as the formation of micro-shorts as copper deposits begin to penetrate the separator. As copper bridges grow, the internal short resistance gradually decreases and a lower magnitude of voltage is required to pass a constant current through the device (in accordance with Ohm's Law).¹³ As the cell reaches Stage IV of the overdischarge, the electrochemical reactions within the cell stabilize and the voltage curve asymptotically approaches a plateau around -0.23 V. At this point, the copper bridges across the cell have grown sufficiently to cause the cell to behave as a resistor in the circuit rather than an electrochemical system, as electrical current is able to pass directly through the cell.

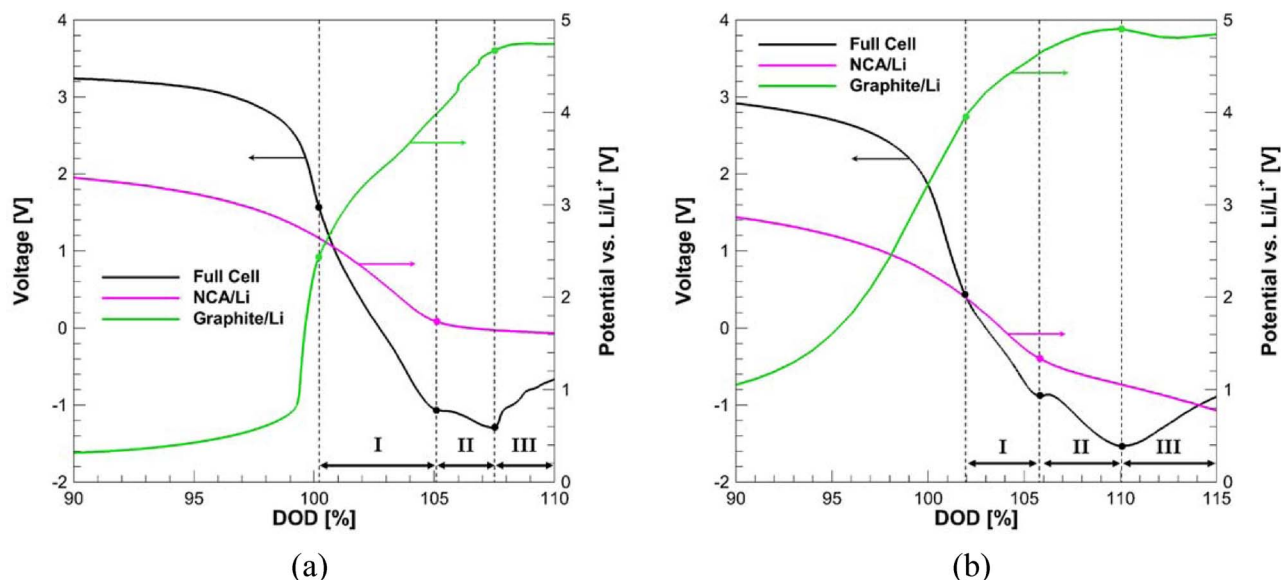


Figure 3. Half cell overdischarge voltage curves for (a) C/10-rate and (b) 1C-rate, aligned with experimental voltage curves from full cells. The processes driving the full cell behavior are decoupled, showing the respective contributions of the cathode and anode to the full cell voltage and to the definitions of Stages I, II, and III.

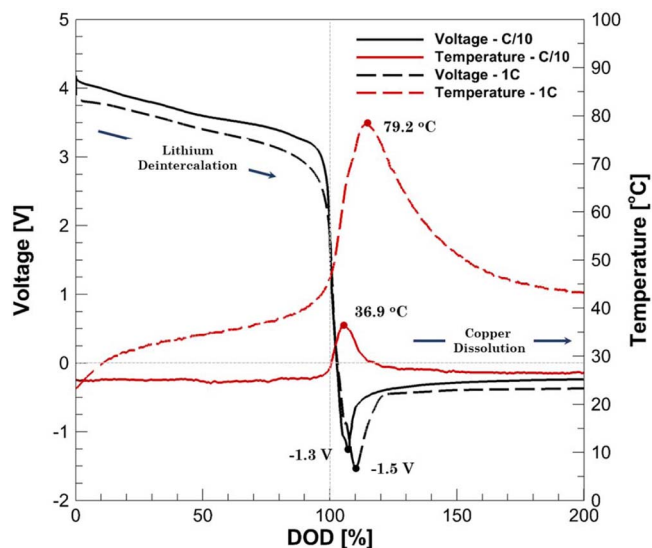


Figure 4. Extreme overdischarge at low (C/10) and high (1C) rate. Electrochemical and thermal response of the cell during the overdischarge test.

The temperature responses, measured by K-type thermocouples on the cell surfaces, are shown alongside their corresponding voltage curves in Figure 4. As expected, surface temperature was found to be highly rate-dependent for the overdischarge process, as the 1C cell reached a maximum temperature of 79.2 °C while the C/10 cell only reached a maximum temperature of 36.9 °C. Temperature begins to increase rapidly around 100% DOD as ionic concentration gradients begin to build in both electrodes near the end of normal discharge. An inflection point in the temperature curve aligns with the initiation of SEI breakdown, showing that this process further increases the heat generation rate. The cell temperature reaches a maximum shortly after the onset of copper dissolution and gradually declined afterwards. This thermal response at both low and high C-rate points out that once the copper substrate starts dissolving, the thermal behavior of the cell is dominated by convection and not by the side copper dissolution reaction. This response also indicates that no threatening thermal

condition arises from the formation of the internal short, showing the relative fail-safe behavior of extreme overdischarge.

Destructive physical analysis was performed on cells that experienced extreme overdischarge so that internal damage to cell components could be analyzed. A depiction of the process used to deconstruct the cells is shown in Figure 5. In order to acquire a baseline for comparing the DPA results, a fresh cell was opened first. The unraveled cathode, anode, and separator surfaces of the fresh cell are shown in Figures 6a and 6b. Both electrodes are double-sided, appearing smooth and black in the discharged state, although anode color varies with state of charge.²² The separator material is white on the anode-facing sides and tan on the cathode-facing sides due to the Al₂O₃ ceramic coating facing the cathode. This coating is intended to improve the thermal stability of the separator and mitigate the consequences of lithium dendrite formation in the cell by preventing internal shorts from penetrating the separator.²³

The anode of the overdischarged cell suffered visible damage; see Figure 6c. Before it was unraveled, the graphite material surface appeared mostly undamaged, but several deep cracks were found in the roll after it was unraveled. The dissolution of the copper current collector greatly reduces the mechanical stability of the anode while subsequently increasing the charge transfer resistance of the cell. Cracking also results in capacity loss and, in extreme cases, loss of electrical connection between the anode and the external circuit. As the anode was unraveled, it was revealed that the remaining copper current collector was extremely thin and unstable. Much of the anode material crumbled under light stress as it was unraveled, leaving large gaps in the roll, as shown in Figure 6c. Meanwhile, the anode-facing separator faces showed essentially no damage or discoloration.

The cathode of the overdischarged cells also showed a visible degradation, Figure 6d. Unlike the anode, the positive electrode did not exhibit any cracks or brittleness. On the contrary, the mechanical stability of the electrode seems to be reinforced due to the presence of the copper on its surface. The cathode active material from the electrode and the ceramic coating from the separator were the elements with the largest instability. Cathode active material showed some detachment from the electrode, while the ceramic coating was detached from the separator. In all cells, the cathode-facing separators facing the exterior of the cell exhibited a predominant detachment of the ceramic coating while the separator facing the center of the cell exhibited a detachment of the cathode active material.

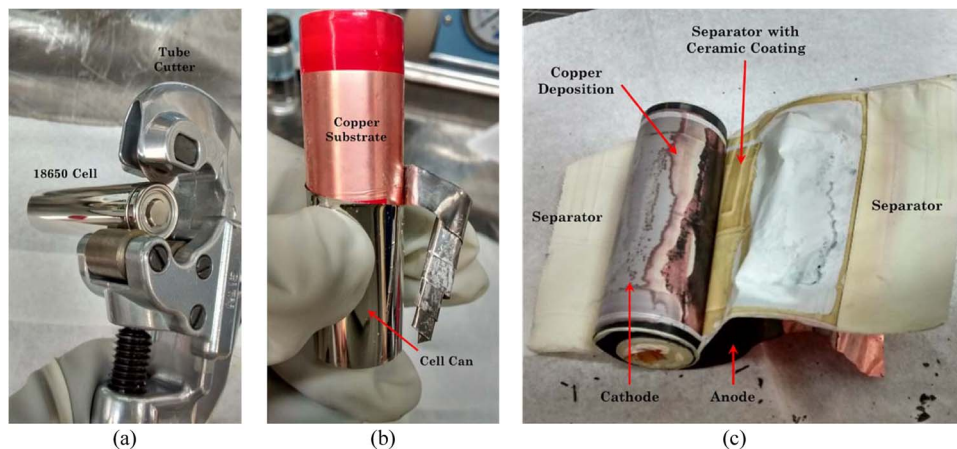


Figure 5. Destruction physical analysis of the overdischarged cell. Process of the disassembly of cells: (a) cell header is removed using a tube cutter, (b) casing is peeled away with needle pliers, and (c) electrodes and separators are unrolled. Externally, the jelly roll did not show any visual damage at naked eye. However, during the electrodes unrolling the negative electrode showed some brittleness and it felled apart by simply touching it.

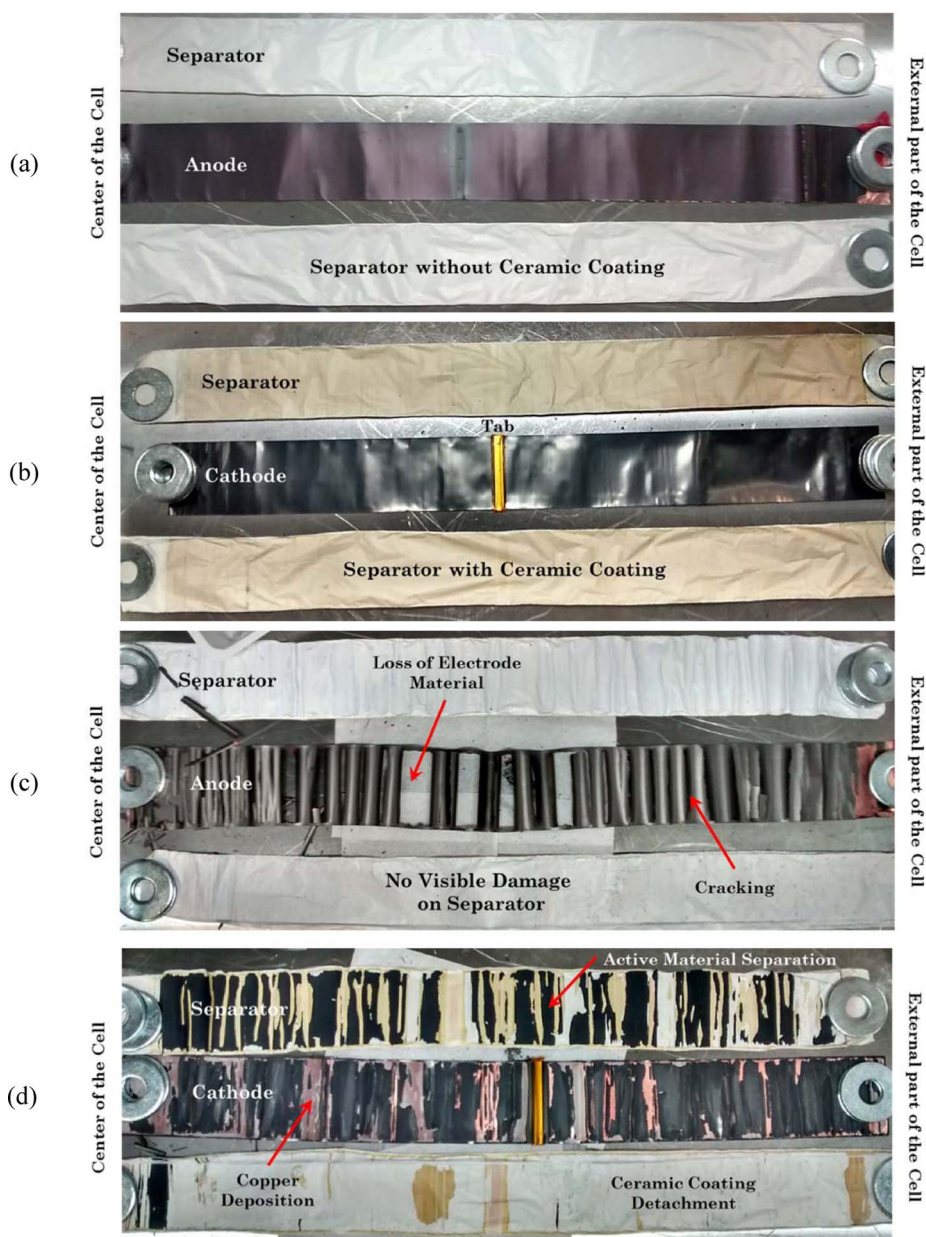


Figure 6. Destructive physical analysis test. Electrodes harvested from a fresh cell (not cycled) and separators facing them: (a) anode, and (b) cathode. Electrodes harvested from the overdischarged cell at 1C-rate. (c) anode, and (d) cathode.

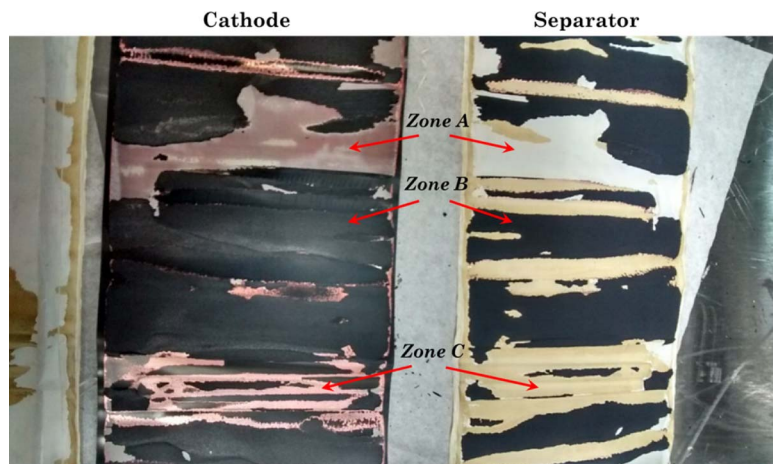


Figure 7. Characteristic electrode degradation zones found close-up center-facing cathode surface, aligned with the corresponding separator. *Zone A*: detachment of ceramic coating from separator. *Zone B*: detachment of cathode active material. *Zone C*: copper deposition on cathode surface without material detachment from either electrode or separator.

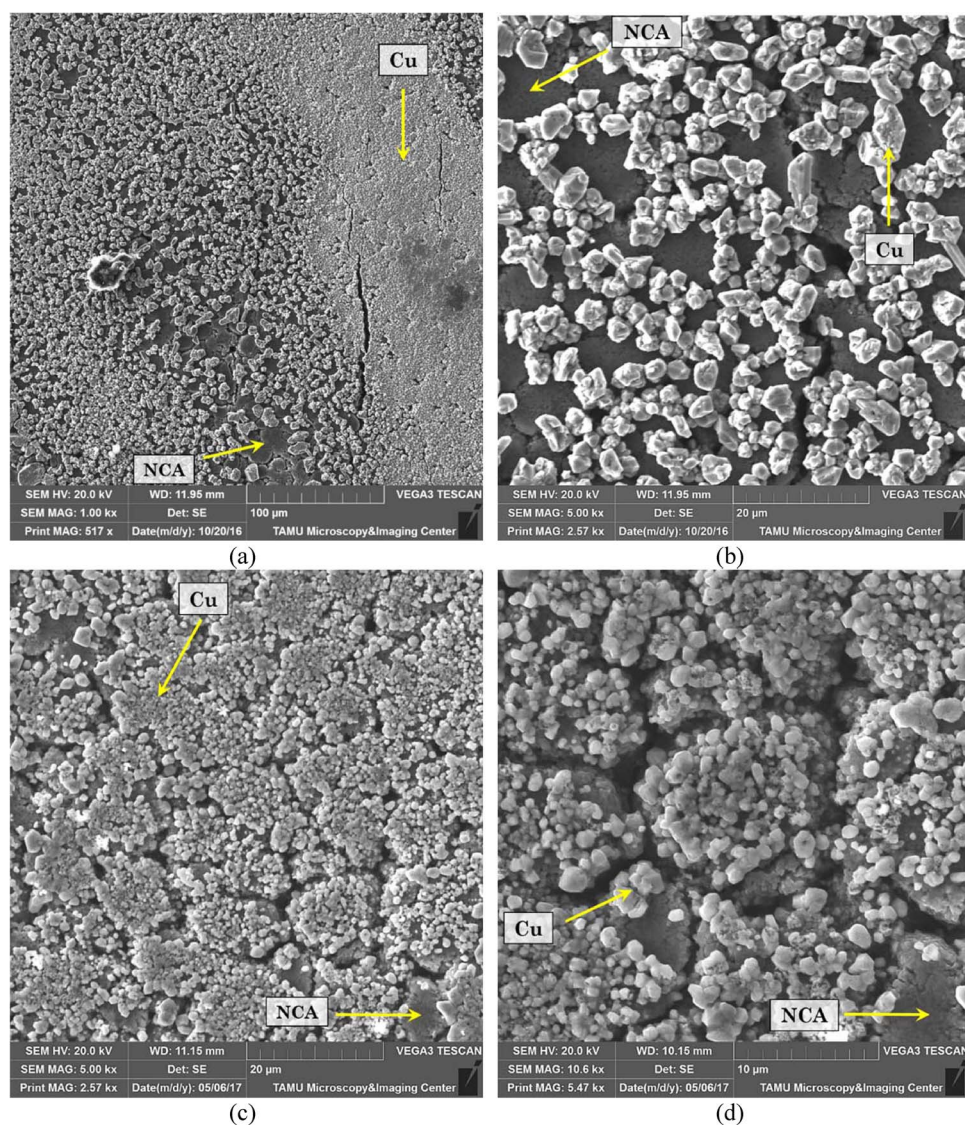


Figure 8. SEM images of cathode surfaces of overdischarged cells. (a) C/10-rate at 1 kX magnification, (b) C/10-rate at 5 kX magnification, (c) 1C-rate at 5 kX magnification, (d) 1C-rate at 10 kX magnification. Copper deposits appear as light-colored particles on the surface.

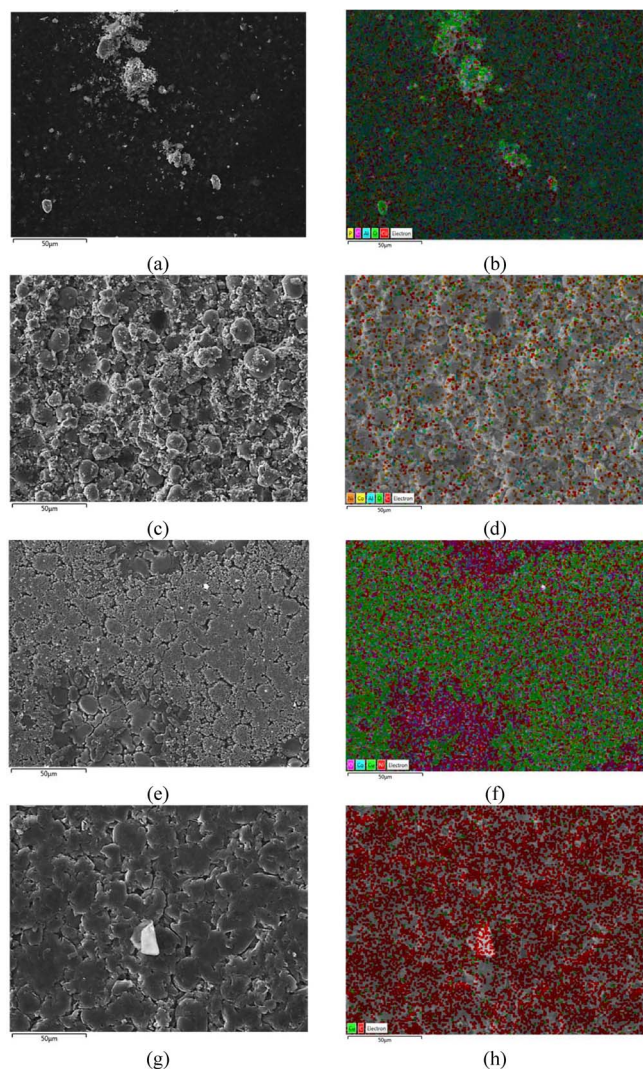


Figure 9. EDS images of the samples extracted from the C/10 extremely overdischarged cell. (a) SEM (1.0 kX) and (b) EDS test of a cathode sample from Zone A: separator ceramic coating adhered to cathode surface. (c) SEM (1.0 kX) and (d) EDS of a cathode sample from Zone B: cathode bulk active material exposed. (e) SEM (1.0 kX) and (f) EDS of a cathode sample from Zone C: cathode surface with a deposited layer of copper. (g) SEM (1.0 kX) and (h) EDS of an anode sample. Percentages of identified elements are listed in Table I.

The center-facing side of the fully unraveled cathode roll and the corresponding separator faces are shown in Figure 7. Extensive damage to both the cathode and separator surfaces is evident due to the non-uniformity and discoloration of the components. The degraded cathode can be divided into three zones, as labeled in the close-up image of Figure 7. In Zone A, the ceramic coating on the separator detached and stuck to the cathode. The coloring of Zone A suggests that a layer of copper below the ceramic is providing the adhesion. In Zone B, a layer of cathode material adhered to the separator, tearing away from the electrode. Zone C represents a region where no material was ripped from either the electrode or separator surface, but a layer of copper deposition is visible. Samples from each of the three zones were taken for SEM and EDS post-mortem analysis to prove the presence of copper.

The cathode surfaces of two overdischarged cells were examined via SEM imaging following the DPA. One cell, shown in Figures 8a and 8b, was overdischarged at a C/10-rate, while the other, shown in Figures 8c and 9d, was overdischarged at a 1C-rate. The most notable difference between these cells is the size of the grains formed

by the copper deposits. In comparing Figures 8b and 8c, each using a magnification of 5 kX, the grains formed in the 1C cell are significantly smaller and appear to be distributed more uniformly across the surface. This result can be explained by nucleation kinetics, as more nuclei tend to form and propagate during high-rate phase formation, resulting in finer grains.²⁴

The results of EDS for the samples extracted from the C/10 overdischarged cell are shown in Table I. The cathode sample from Zone A, see Figures 9a and 9b, represents a region where the separator coating adhered to the cathode surface as the cathode and separator were peeled apart during DPA. This sample contained large amounts of copper, carbon, oxygen, and aluminum. The high concentration of aluminum and oxygen indicate that the ceramic coating of the separator was present on this surface. Fluorine and phosphorus are both present in the cell's electrolyte in the form of LiPF_6 , and thus both elements should be embedded in the separator material. The presence of 22.6% copper by weight confirms that copper deposition occurs in the separator material as well as on the cathode surface. Zone B represents a region where the surface of the cathode material was torn away and the bulk active material was exposed, as seen in Figures 9c and 9d. In this region, neither copper nor the elements of the electrolyte were present, indicating that copper was deposited primarily on the cathode surface rather than intercalating into the matrix. In Zone C, the cathode surface was left intact, but was coated with a layer of copper, as seen in Figures 9e and 9f. EDS results indicate that this region contained 47.9% copper by weight, confirming that the cathode surface was the preferred location for copper deposition. A sample from the anode surface was also tested, see Figures 9g and 9h, and it was discovered that this surface contained 3.5% copper by weight. The presence of copper deposits on both electrode surfaces, as well as within the separator, indicates that an internal short was formed in the cell. Although internal shorting can be consistently induced through deep overdischarge, as suggested by Guo et al., this method does not realistically simulate the dangers of internal shorting during cell operation because the stored energy in a cell at the end of a deep overdischarge phase is minimal. Since the magnitude of the final voltage plateau is small for both discharge rates, the power through the short remains low ($P = iV$) and the heat produced is safely dissipated in the cell. Although localized heating and evaporation of the electrolyte can be a concern when passing current directly through an internal short, no swelling or venting was observed in these tests.

Conclusions

The results of the overdischarge test showed that extreme overdischarge conditions can lead to the dissolution of copper from the anodic current collector, which can lead to severe capacity loss and the deposition of metallic copper on the surface of the cathode, anode, and the cathode-facing separator surfaces. Cells under test were found to be prone to failure due to blockage of the cathode's reactive surface by the deposited copper, an increase in charge transfer resistance between the anode and external circuit due to cracking in the copper current collector, and the formation of copper bridges that internally short the cell.

Previous studies report that heat generation will occur during attempted cycling after overdischarge, as the blockage of electrode surfaces by copper prevents lithium ions from intercalating and causes them to deposit as lithium metal dendrites.²⁵ These dendrites can then cause localized heating, venting, and thermal runaway upon repeated cycling. Additionally, the re-oxidation of some of the deposited copper can compete with the intended oxidation of lithium, greatly hindering cell performance.¹⁶ In this study, only a deep overdischarge phase was studied and no dangerously high temperatures were observed, even under extreme overdischarge conditions. This indicates that internal shorting due to the formation of copper dendrites in overdischarged cells is not a catastrophic event until recharge is attempted. Internally shorted cells in a large bank of cells can be dangerous because large amounts of heat are generated during the attempted recharge of a shorted cell. Additionally, the voltage unbalance created by one

Table I. Elemental composition of samples extracted from the C/10 overdischarged cells obtained via EDS.

Sample			Composition (wt%)							
Electrode	Zone	Description	Cu	C	O	Ni	Co	Al	F	P
Cathode	A	Separator adhesion	22.6	23.5	22.0	4.6	1.4	16.4	6.9	2.6
Cathode	B	Removed cathode material	0.0	42.4	13.7	31.8	6.4	2.4	0.0	0.0
Cathode	C	Exposed copper	47.9	0.0	14.0	27.8	5.8	0.8	2.8	0.0
Anode	-	Graphite surface	3.5	95.7	0.0	0.0	0.0	0.0	0.0	0.8

overdischarged cell bank can cause other banks in series to experience an overcharge condition in successive cycles.²⁵ In severe cases, the heat generation can lead to thermal runaway and can cause the cell to catch fire or explode, putting neighboring cells at risk. Therefore, cells that experience copper dissolution in modules should be immediately replaced upon detection.

Heat generation in the cells mainly occurred before the initiation of copper dissolution and is attributed to concentration polarization in the cell at the end of its discharge phase, as well as the breakdown of the SEI layer. The cell that was overdischarged at a 1C rate experienced surface temperatures as high as 79°C. Peak surface temperature was found to be highly rate-dependent, although it is believed that thermal runaway is unlikely to be a threat in a single-cell setup even at high rates of discharge. Although the phenomenon of copper dissolution in extreme overdischarge of Li-ion batteries was found to be a relatively benign failure mode, this study elucidates the mechanisms of the entire overdischarge process and demonstrates the need for balancing and monitoring systems in the design of large battery packs and modules, as one cell with an unbalanced voltage can lead to dangerous consequences for the whole battery system.

Acknowledgment

This work was supported by Underwriters Laboratories Inc. The authors acknowledge the facilities and technical assistance of the Microscopy and Imaging Center (MIC) at Texas A&M University (TAMU). Mukherjee group moved from TAMU to Purdue University. CF and DJR contributed equally to this work.

ORCID

Partha P. Mukherjee  <https://orcid.org/0000-0001-7900-7261>

References

- R. A. Huggins, *Advanced Batteries: Materials Science Aspects*, Springer Science + Business Media, LLC (2009).
- V. Etacheri, R. Marom, R. Elazari, G. Salitra, and D. Aurbach, *Energy Environ Sci*, **4**, 3243 (2011).
- C. Chanson and J.-P. Wiaux, *Safety of Lithium-ion batteries*, in, p. 10, RECHARGE aisbl, Brussels, Belgium (2013).
- B. Jansen, *Crash investigators trace UPS plane fire to batteries*, in USA Today, Online (2013).
- S. Tibken and R. Cheng, *Samsung answers burning Note 7 questions, vows better batteries*, in CNET, Online (2017).
- C. Matyszczyk, *Dell laptop explodes again and again and again*, in CNET, Online (2017).
- D. P. Finegan, M. Scheel, J. B. Robinson, B. Tjaden, M. Di Michiel, G. Hinds, D. J. L. Brett, and P. R. Shearing, *Phys. Chem. Chem. Phys.*, **18**, 30912 (2016).
- T. Waldmann, A. Iturrondobeitia, M. Kasper, N. Ghanbari, F. Aguesse, E. Bekaert, L. Daniel, S. Genies, I. J. Gordon, M. W. Loble, E. De Vito, and M. Wohlfahrt-Mehrens, *J. Electrochem. Soc.*, **163**, A2149 (2016).
- C. F. Lopez, J. A. Jeevarajan, and P. P. Mukherjee, *J. Electrochem. Soc.*, **162**, A2163 (2015).
- H. He, Y. Liu, Q. Liu, Z. Li, F. Xu, C. Dun, Y. Ren, M.-x. Wang, and J. Xie, *J. Electrochem. Soc.*, **160**, A793 (2013).
- H. Lee, S.-K. Chang, E.-Y. Goh, J.-Y. Jeong, J. H. Lee, H.-J. Kim, J.-J. Cho, and S.-T. Hong, *Chem. Mat.*, **20**, 5 (2007).
- J. Chen, C. Buhrmester, and J. R. Dahn, *Electrochem. Solid St. Lett.*, **8**, A59 (2005).
- R. Guo, L. Lu, M. Ouyang, and X. Feng, *Scientific Reports*, 30248 (2016).
- H. Maleki and J. N. Howard, *J. Power Sources*, **160**, 1395 (2006).
- E. J. Nemanick, D. Wang, J. Matsumoto, and N. Ives, in *230th ECS Meeting*, Honolulu, HI (2016).
- H. F. Li, J. K. Gao, and S. L. Zhang, *Chinese J Chem*, **26**, 1585 (2008).
- C. Kishiyama, M. Nagata, T. Piao, J. Dodd, P. Lam, and H. Tsukamoto, in *204th Electrochemistry Society Conference*, Orlando, FL (2003).
- Z. Mao, in *206th Electrochemistry Society Conference*, Honolulu, HI (2006).
- J. Kasnatscheew, M. Borner, B. Streipert, P. Meister, R. Wagner, I. Laskovic, and M. Winter, *J. Power Sources*, **362**, 278 (2017).
- K. Park, J. H. Cho, K. Shanmuganathan, J. Song, J. Peng, M. Gobet, S. Greenbaum, C. J. Ellison, and J. B. Goodenough, *J. Power Sources*, **263**, 52 (2014).
- M. Stein IV, C.-F. Chen, D. Juarez-Robles, C. Rhodes, and P. P. Mukherjee, *J. Vis. Exp.*, (108), e53490 (2016).
- P. Maire, A. Evans, H. Kaiser, W. Scheifele, and P. Novak, *J. Electrochem. Soc.*, **155**, A862 (2008).
- J.-A. Choi, S. H. Kim, and D.-W. Kim, *J. Power Sources*, **195**, 6192 (2010).
- L. Guo, G. Oskam, A. Radisic, P. Hoffmann, and P. Searson, *J. Phys. D - Appl. Phys.*, **44**, 443001 (2011).
- Y. Zheng, K. Qian, D. Luo, Y. Li, Q. Lu, B. Li, Y. He, X. Wang, J. Li, and F. Kang, *Rsc Advances*, **6**, 30474 (2016).